# Kinematic Analysis of a Novel Humanoid Wrist Parallel Mechanism

Christoph Stoeffler, Adriano del Rio Fernandez, Heiner Peters, Moritz Schilling, and Shivesh Kumar

**Abstract** Wrist mechanisms in humanoid robots play a crucial role by fundamentally influencing the dexterity of robotic hands. Recent designs often exploit parallel mechanisms due to their ability to transmit high loads while offering the possibility to minimize peripheral inertia of the arms. This often comes at the cost of reduced workspace. In this paper, a novel wrist mechanism of type $2SU[RS\underline{P}U] + 1U$ is presented, with the aim to achieve human-like range of motion with good force transmission capabilities in a compact form. An in-depth kinematic analysis of the new parallel mechanism is presented including solutions to both forward and inverse kinematics and a comparison to the traditional $2S\underline{P}U + 1U$ mechanism is drawn, showing increased dexterity and range of motion.

## 1 Introduction

A common approach in robotics is to tailor the robot's joint modules specifically to their intended tasks. This functional design becomes even more relevant for humanoids, since they possess a complex structure where different parts take different specific tasks, such as walking, grasping, or manipulating. In [8], it is argued that human muscle structures can be considered generally parallel. Recently, parallel kinematic machines (PKMs) found many applications for joint modules in humanoid robots, due to their ability to transmit motor motions non-linearly to the relevant joints (see [9] for a survey). Many different wrist designs have been proposed in the robotics community, where the majority focused on 2-DOF mechanisms - see [7]. Notably, the $2S\underline{P}U + 1U$-topology is often used (e.g. wrist joint in RH5 humanoid [1]) and has

Christoph Stoeffler and Adriano del Rio Fernandez
Bremen University Bremen, Germany, e-mail: stoeffle@uni-bremen.de

Heiner Peters, Moritz Schilling and Shivesh Kumar
German Research Center for Artificial Intelligence, Robotics Innovation Center, Bremen, Germany
e-mail: firstname.lastname@dfki.de

for example been extended in [6] for humanoid ankle application. Such mechanisms fall in the class of parallel mechanisms with actuation legs and motion constraint generator legs (see [5] for an extensive study on their synthesis). These designs still suffer from a limited range of motion. In this paper, we present the kinematic analysis

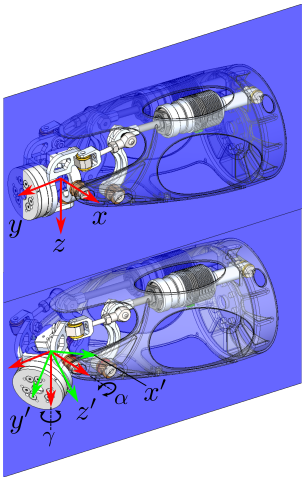


(a) Mechanical design of the new $2SU[RS\underline{P}U] + 1U$-mechanism for a humanoid wrist. Due to its symmetry, inverse kinematic descriptions are carried out on one side of the depicted half-plane.

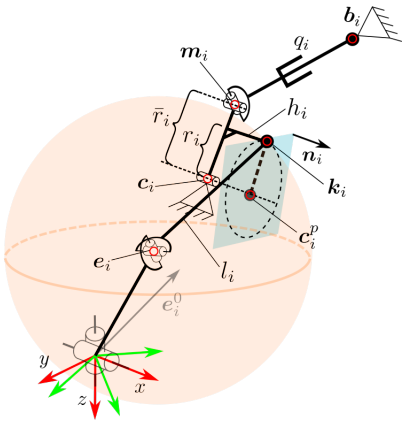


(b) Geometric parameters used in the computation of kinematic relations. Here, one half of the mechanism is depicted by cutting along the $y-z$-axis (see Fig. 1a).

Fig. 1: CAD depiction of new wrist and its schematic

of a novel parallel mechanism of type $2SU[RS\underline{P}U] + 1U$ for implementing the wrist joint of RH5v2 humanoid (see Fig. 1a) which overcomes the restricted range of motion of traditional $2S\underline{P}U + 1U$ design used in RH5 humanoid. The mechanism offers increased workspace for *flexion* and *extension* of the hand with a special focus on increasing the flexion capability of the wrist. This mechanism was first employed by the authors in the robotic system *Charlie* [3] as an ankle joint. However, an in-depth analysis of this mechanism is missing in the literature. We present the inverse, forward and differential kinematics solution of this novel mechanism. It is demonstrated that this mechanism can have a maximum of 4 solutions to its inverse kinematics and 8 solutions to the forward kinematics problems. Further, using the differential kinematics, the dexterity analysis of the proposed mechanism is performed and the design is compared with traditional $2S\underline{P}U + 1U$ design.

## 2 Architecture and Constraint Equations

Figure 1a shows the CAD design and Figure 1b shows the mechanism's schematic. It exhibits $n = 4 \times 2 + 1 + 1 = 10$ bodies and $m = 6 \times 2 + 1 = 13$ joints that posses $f_{tot} = 26$ degrees of freedom. Applying the *Grübler-Kutzbach criteria* for spatial mechanisms yields

$$M = 6(n - m - 1) + \sum f_i = 6(10 - 13 - 1) + 26 = 2$$

degrees of freedom for the proposed design. The wrist therefore allows movements around the $x$- and $y$-axis that we denote subsequently with *inclination* ($\alpha$) and *tilt* ($\gamma$). The underlying constraint equations of the mechanism are based on the points

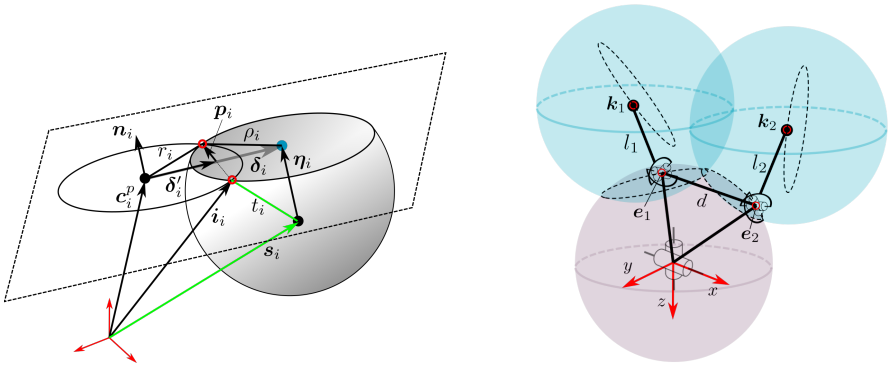


(a) Circle-sphere intersection that can be brought to a circle-circle intersection by projection.

(b) Forward geometric problem: While $\mathbf{k}_1$ and $\mathbf{k}_2$ lie themselves on circles, the cranks $l_1$ and $l_2$ span spheres that intersect with the sphere emerging from end-effector rotation.

Fig. 2: Geometric details to solve the inverse and forward kinematics

$\boldsymbol{k}_i$, that are likewise constrained by actuator lengths and end-effector configuration. Our developments are generally given for both sides of the mechanism (see Fig. 1a), such that $i \in \{1, 2\}$

$$\left\| \mathbf{c}_i + \frac{\bar{r}_i}{r_i}(\mathbf{k}_i - \mathbf{c}_i^p) - \mathbf{b}_i \right\|^2 - q_i^2 = 0 \tag{1}$$

$$h_i := \left\| \boldsymbol{R}(\alpha, \gamma)\mathbf{e}_i^0 - \mathbf{k}_i \right\|^2 - l_i^2 = 0 \tag{2}$$

where vectors and scalars are depicted in Fig. 1b. The rotation matrix $\boldsymbol{R}(\alpha, \gamma)$ is parameterized by inclination $\alpha$ and tilt $\gamma$. It can generally be of *intrinsic* or *extrinsic* type, employing the matrices $\boldsymbol{R}_z(\gamma)\boldsymbol{R}_x(\alpha)$ or $\boldsymbol{R}_z(\alpha)\boldsymbol{R}_x(\gamma)$, respectively.

## 3 Kinematics

Computing the forward and inverse kinematics involves to solve for $\boldsymbol{k}_i$, what can be achieved by considering the general problem of a circle-sphere intersection and is depicted in Fig. 2a. Formally, it writes $C(\mathbf{c}_i^p, \mathbf{n}_i, r_i) \cap \mathcal{S}(\mathbf{s}_i, t_i) \rightarrow \mathbf{i}_i^+, \mathbf{i}_i^-$, where $r_i$, $\mathbf{n}_i$ and $\mathbf{c}_i^p = \mathbf{c}_i + h_i \mathbf{n}_i$ can be taken from Fig. 1b. By exploiting the dot product together with a scalar multiplication, the vector $\boldsymbol{\eta}_i = \left((\mathbf{c}_i^p - \mathbf{s}_i) \cdot \mathbf{n}_i\right) \mathbf{n}_i$ can be computed which points from $\mathbf{s}_i$ to the plane of intersection. This reduces the problem to a circle-circle intersection and the circle radius the intersected sphere is given by $\rho_i^2 = t_i^2 - \boldsymbol{\eta}_i \cdot \boldsymbol{\eta}_i$. The distance vector between both circle centers is simply obtained by $\boldsymbol{\delta}_i = \mathbf{s}_i + \boldsymbol{\eta}_i - \mathbf{c}_i^p$ as depicted in Fig. 2a. The distance to the line of intersecting points, together with component that accounts for its direction, is then computed by

$$\boldsymbol{\delta}_i' = \frac{\boldsymbol{\delta}_i \cdot \boldsymbol{\delta}_i + r_i^2 - \rho_i^2}{2||\boldsymbol{\delta}_i||} \frac{\boldsymbol{\delta}_i}{||\boldsymbol{\delta}_i||} = \frac{\boldsymbol{\delta}_i}{2} + \boldsymbol{\delta}_i \frac{r_i^2 - \rho_i^2}{2\boldsymbol{\delta}_i \cdot \boldsymbol{\delta}_i} = \frac{\boldsymbol{\delta}_i}{2} + \boldsymbol{\delta}_i \frac{r_i^2 - t_i^2 + \boldsymbol{\eta}_i \cdot \boldsymbol{\eta}_i}{2\boldsymbol{\delta}_i \cdot \boldsymbol{\delta}_i}.$$

Additionally, the orthogonal vector to $\boldsymbol{\delta}_i'$ that is pointing to the intersection points and being of length $\sqrt{r_i^2 - \boldsymbol{\delta}_i' \cdot \boldsymbol{\delta}_i'}$ is computed by using the planes normal vector $\mathbf{n}_i$:

$$\mathbf{p}_i = \frac{\boldsymbol{\delta}_i'}{||\boldsymbol{\delta}_i'||} \times \mathbf{n}_i \sqrt{r_i^2 - \boldsymbol{\delta}_i' \cdot \boldsymbol{\delta}_i'}. \tag{3}$$

Finally, two intersection points are obtained with

$$\mathbf{i}_i = \mathbf{c}_i^p + \boldsymbol{\delta}_i' \pm \mathbf{p}_i. \tag{4}$$

Inserting $\mathbf{k}_i^+, \mathbf{k}_i^- \leftarrow C(\mathbf{c}_i^p, \mathbf{n}_i, r_i) \cap \mathcal{S}(\boldsymbol{R}(\alpha, \gamma)\mathbf{e}_i^0, l_i)$ into Equ. 1 and rearranging for $q_i$ gives the solution of inverse kinematics problem. According to the circle-sphere intersection for computing the positions of $\boldsymbol{k}_i$, there exist four inverse solutions to the mechanism that are shown in Fig.3. Determining the forward kinematics - that

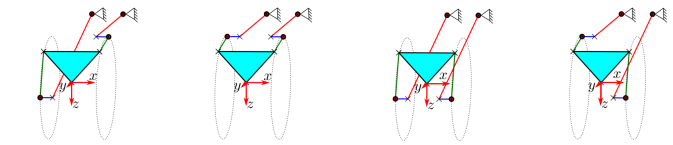

(a) $q_1 = 0.133\,\mathrm{m}$, $q_2 = 0.200\,\mathrm{m}$ (b) $q_1 = 0.133\,\mathrm{m}$, $q_2 = 0.133\,\mathrm{m}$ (c) $q_1 = 0.200\,\mathrm{m}$, $q_2 = 0.200\,\mathrm{m}$ (d) $q_1 = 0.200\,\mathrm{m}$, $q_2 = 0.133\,\mathrm{m}$

Fig. 3: Inverse solutions for the configuration $\alpha = 0$ and $\gamma = 0$. Dashed circles indicate the constraints arising from the revolute joints located in $\boldsymbol{c}_i$.

is computing the wrist orientation from actuator inputs $q_i$ - presents itself to be more involving. In a first step, the already explained circle-sphere intersection can be exploited again to obtain $\mathbf{m}_i^+, \mathbf{m}_i^- \leftarrow C(\mathbf{c}_i^p, \mathbf{n}_i, r_i) \cap \mathcal{S}(\mathbf{b}_i, q_i)$ what translates into

$$\mathbf{k}_i = \mathbf{c}_i + \frac{r_i}{\bar{r}_i}(\mathbf{m}_i - \mathbf{c}_i) + h_i \mathbf{n}_i. \tag{5}$$

Once the spatial locations of $\mathbf{k}_i$ are known, the remaining geometric problem to solve, consists of two sphere-sphere intersections, as to be seen in Fig 2b. By means of *Gröbner Bases* of the ideal $\mathcal{I} = \langle h_1, h_2, h_3, h_4 \rangle | \mathcal{I} \subseteq k[t, u, v, w]$ one can solve the system of nonlinear equations, defined by Equ. 2 and augmented by the parametrization of rotations:

$$h_3 := t^2 + u^2 - 1 = 0 \qquad \text{where} \quad t = \cos(\alpha),\ u = \sin(\alpha), \tag{6}$$

$$h_4 := v^2 + w^2 - 1 = 0 \qquad \text{where} \quad v = \cos(\gamma),\ w = \sin(\gamma). \tag{7}$$

The software *Maple* was used to sample through the feasible actuation space (see Tab. 2) to compute Gröbner bases of the above ideal, revealing a univariate polynomial of degree 8. With four solutions for $\mathbf{k}_i$, a maximum of 8 real forward solutions were computed and are depicted in Fig. 4. For the plots of this section and of Sec. 4[1], the assembly mode of the designed wrist mechanism of Fig. 1a is used for computations. Its geometric parameters are listed in Tab. 1. With the closed-form solution to

Table 1: Geometric data of the build wrist with variables defined in Fig. 1a - all values in [m], except for $\boldsymbol{n}_i$

| | |
|---|---|
| $\boldsymbol{b}_1 = [0.015 \quad -0.178 \quad -0.034]^T$ | $\boldsymbol{b}_2 = [-0.015 \quad -0.178 \quad -0.034]^T$ |
| $\boldsymbol{c}_1 = [0.015 \quad -0.032 \quad 0.011]^T$ | $\boldsymbol{c}_2 = [-0.015 \quad -0.032 \quad 0.011]^T$ |
| $\boldsymbol{e}_1^0 = [0.027 \quad 0 \quad -0.03]^T$ | $\boldsymbol{e}_2^0 = [-0.027 \quad 0 \quad -0.03]^T$ |
| $\boldsymbol{n}_1 = [1 \quad 0 \quad 0]^T$ | $\boldsymbol{n}_2 = [-1 \quad 0 \quad 0]^T$ |
| $\hat{r}_i = 0.049, \quad r_i = 0.049,$ | $h_i = 0.012, \quad l_i = 0.045$ |

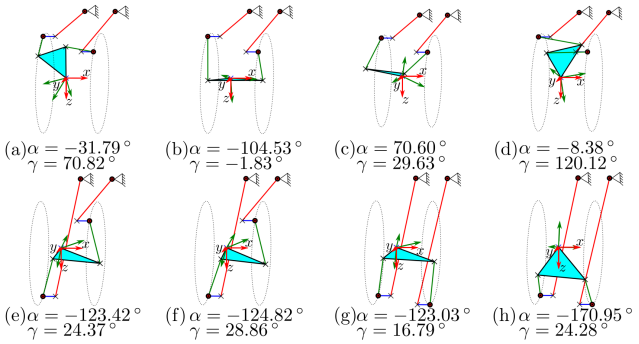


Fig. 4: Forward solutions for the actuator length $q_1 = 0.155\,\text{m}$ and $q_2 = 0.178\,\text{m}$. Dashed circles indicate the constraints arising from the revolute joints located in $\boldsymbol{c}_i$.

[1] Software implementations will be made available upon acceptance of paper

inverse kinematics problem, the constraint Jacobian of the mechanism can be computed, which reveals information about workspace conditioning and singularities. Equ. 1 can be brought into the form $\boldsymbol{g}(\boldsymbol{x},\boldsymbol{q}) = \boldsymbol{0}$, differentiation then yields

$$\frac{\partial \boldsymbol{g}(\boldsymbol{x},\boldsymbol{q})}{\partial \boldsymbol{x}}\dot{\boldsymbol{x}} = -\frac{\partial \boldsymbol{g}(\boldsymbol{x},\boldsymbol{q})}{\partial \boldsymbol{q}}\dot{\boldsymbol{q}} \Leftrightarrow \dot{\boldsymbol{x}} = -\boldsymbol{J}_x^{-1}\boldsymbol{J}_q\dot{\boldsymbol{q}} = \boldsymbol{J}\dot{\boldsymbol{q}} \tag{8}$$

where the Jacobian $\boldsymbol{J}$ is the product of the inverted *work space Jacobian* $\boldsymbol{J}_x$ and the *joint space Jacobian* $\boldsymbol{J}_q$. The condition index or determinant of the Jacobian (see e.g. [2]) can be used to quantify the mechanism, since its input and output spaces are $\mathbb{R}^2$ and $SO(3)$ respectively.

## 4 Performance Analysis

In Fig. 5 the condition index and singularities of the novel mechanism are shown. While the universal joint of the end-effector can theoretically reach $\alpha, \gamma \in [-\pi, \pi]$, additional constraints of the linkages restrict the workspace and no kinematic solution exists in the white areas. Actuator limits (see Tab. 2) further restrict motion to the dashed area. To highlight mechanism improvements, we propose a simple $2S\underline{P}U +$

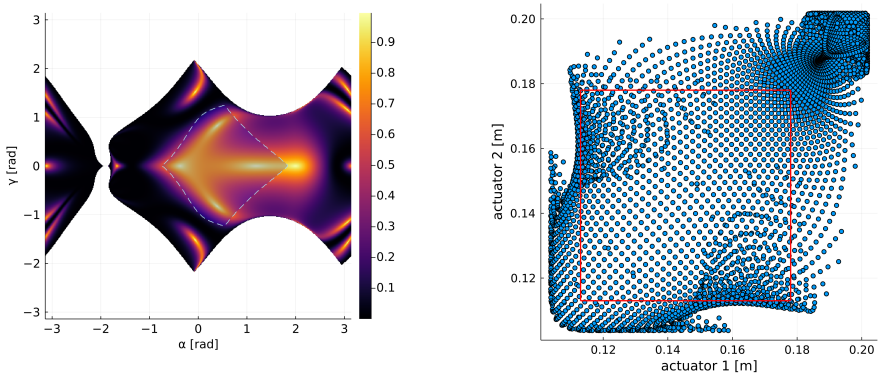


(a) Conditioning of the build mechanism, determined with $1/\mathrm{cond}(\boldsymbol{J}\boldsymbol{J}^T)$.

(b) Configuration space of the mechanism with actuator limits

Fig. 5: Dexterity measure and singularities in task space of the novel wrist

$1U$-mechanism as a design to compare against, with the linear actuators acting directly on the end-effector platform. In analogy to the novel mechanism, the inverse kinematics and Jacobian for the $2S\underline{P}U + 1U$ design can be computed by rearranging and differentiating $g_i^c = q_i^2 - \left\|\boldsymbol{R}(\alpha,\gamma)\mathbf{e}_i^0 - \mathbf{b}_i\right\|^2$, respectively. Fig. 6a and 6b show differences in the condition indices of the mechanisms and their singularity curves,

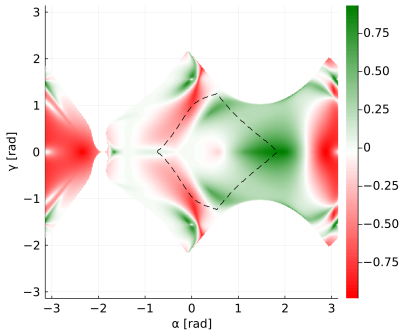


(a) Difference of condition index between new wrist and comparative design. Positive areas indicate that the novel wrist has superior dexterity.

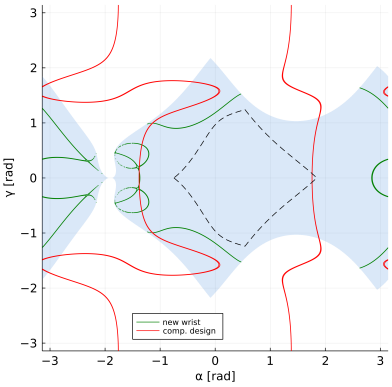


(b) Singularity curves of new wrist and comparative design, showing reduced workspace for the new wrist by grey area.

Fig. 6: Comparison between $2SU[RS\underline{P}U] + 1U$ and $2S\underline{P}U + 1U$ mechanism

respectively. It can be noted that the novel design shows similar dexterity for pure

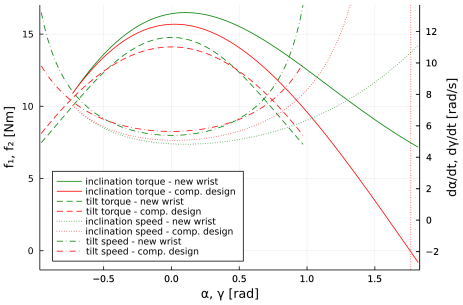


Fig. 7: Torques and speeds for pure inclination ($\gamma = 0$) and pure tilt ($\alpha = 0$).

Table 2: Mechanism specifications and comparative human data [10], [4]. Actuator force and speed refer to the rated ones and rotational speeds are those obtained in the configuration of maximal torques.

| | range | force | speed |
|---|---|---|---|
| **lin. actuators** | 113-178 mm | 262 N | 152 mm/s |
| **incl.** ($\gamma = 0$) | -42/105 deg | 12/17 Nm | 277 deg/s |
| **tilt** ($\alpha = 0$) | -56/56 deg | 12/15 Nm | 309 deg/s |

| comparisons | | (max.) | |
|---|---|---|---|
| **human incl.** | -78/95 deg | 25 Nm | n.a. |
| **human tilt** | -48/37 deg | 7 Nm | n.a. |
| **incl.** $2S\underline{P}U + U$ | -42/101 deg | -2/16 Nm | 291 deg/s |
| **tilt** $2S\underline{P}U + U$ | -56/56 deg | 8/14 Nm | 323 deg/s |

tilt movements under zero inclination angle. However, the design aim of increased dexterity for high inclination angles ($\gamma = 0, 1 \leq \alpha \leq 2$) is clearly met. Additionally, the singularity occurring at positive inclination angles is considerably shifted to higher values in the novel design. Due to limitations in the construction space, the work space was not shifted further in positive tilt direction in this specific application, although this would have been advantageous in terms of dexterity. Finally, Fig. 7 gives an overview of maximal speed and torque in task space under given actuator

input and is complemented by Tab. 2. The novel mechanism is closer to the maximal torques in humans and delivers sufficient torque at high tilt angles.

## 5 Conclusion

In this work, a novel wrist design in the class of parallel 2-DOF mechanisms has been introduced. A closed-form solution of the inverse kinematics and a Gröbner bases approach for the forward kinematics has been presented. This is followed by a performance analysis of the wrist, showing increased dexterity and enlarged workspace compared to a classical 2-DOF mechanism. The here presented design can therefore be a suitable candidate for linkages where an extended inclination angle under good manipulability is required.

**Acknowledgements** This work was partially supported from the projects VeryHuman (FKZ 01IW20004) and TransFIT (FKZ 50RA1701) funded by the German Aerospace Center (DLR) with federal funds from the Federal Ministry of Education and Research (BMBF) and Federal Ministry of Economic Affairs and Energy (BMWi) respectively.

## References

1. J. Eßer et al., "Design, analysis and control of the series-parallel hybrid RH5 humanoid robot," 2020 IEEE-RAS 20th International Conference on Humanoid Robots (Humanoids), 2021, pp. 400-407, doi: 10.1109/HUMANOIDS47582.2021.9555770.
2. Merlet, J.P.: Jacobian, manipulability, condition number and accuracy of parallel robots. Proceedings of 12th International Symposium of Robotics Research (2005)
3. Kuehn, D., Schilling, M., Stark, T., Zenzes, M., Kirchner, F.: System Design and Testing of the Hominid Robot Charlie. Journal of Field Robotics (2016) doi: 10.1002/rob.21662
4. Plewa, K., Potvin, J.P., Dickey, J.P.: Wrist rotations about one or two axes affect maximum wrist strength. Applied Ergonomics **53**, 152–160 (2016)
5. Kuo, C.H. and Dai, J.S., 2013. Task-oriented structure synthesis of a class of parallel manipulators using motion constraint generator. Mechanism and Machine Theory, 70, pp.394-406.
6. Kumar, S., Nayak, A., Peters, H., Schulz, C., Müller, A., Kirchner, F.: Kinematic analysis of a novel parallel 2SPRR+1U ankle mechanism in humanoid robot. Advances in Robot Kinematics, 431–439 (2018)
7. Bajaj, N.M., Spiers, A. J., Dollar, A.M.: State of the Art in Artificial Wrists: A Review of Prosthetic and Robotic Wrist Design. IEEE Transactions on Robotics (2019) doi: 10.1109/TRO.2018.2865890
8. Ceccarelli, M., Russo, M., Morales-Cruz, C.: Parallel Architectures for Humanoid Robots. Robotics (2020) doi: 10.3390/robotics9040075
9. Kumar, S., Wöhrle, H., de Gea Fernández, J., Müller, A. and Kirchner, F., 2020. A survey on modularity and distributivity in series-parallel hybrid robots. Mechatronics, 68, p.102367.
10. Christensen, J.M., McBarron, J.W., McConville, J.T., Pogue, W.R., Williges, R.C., Woodson, W.E.: Man-Systems Integration Standards NASA-STD-3000, Vol. II Rev. B, (1995)